Biogeosciences Discuss., 12, 5503–5533, 2015
www.biogeosciences-discuss.net/12/5503/2015/
doi:10.5194/bgd-12-5503-2015
© Author(s) 2015. CC Attribution 3.0 License.

Biogeosciences Discussions
Open Access

This discussion paper is/has been under review for the journal Biogeosciences (BG).
Please refer to the corresponding final paper in BG if available.

Seasonal variation in vegetation water content estimated from proximal sensing and MODIS time series in a Mediterranean Fluxnet site

G. Mendiguren[1,2,3,4], **M. P. Martín**[2,4], **H. Nieto**[5], **J. Pacheco-Labrador**[2,4], **and S. Jurdao**[4,6]

[1]Geological Survey of Denmark and Greenland (GEUS), Øster Voldgade 10, 1350 Copenhagen K, Denmark
[2]Instituto de Economía, Geografía y Demografía, Centro de Ciencias Humanas y Sociales, Consejo Superior de Investigaciones Científicas (CSIC), Albasanz 26–28, 28037, Madrid, Spain
[3]Department of Geosciences and Natural Resource Management, University of Copenhagen, Øster Voldgade 10, 1350, Copenhagen K, Denmark
[4]Associated Research Unit GEOLAB[2&6]
[5]Instituto de Agricultura Sostenible, Consejo Superior de Investigaciones Científicas (CSIC), 14080 Córdoba, Spain
[6]Department of Geography and Geology, University of Alcalá. Calle Colegios 2, 28801, Alcalá de Henares, Spain

Received: 16 February 2015 – Accepted: 13 March 2015 – Published: 13 April 2015

Correspondence to: G. Mendiguren (gmg@geus.dk)

Published by Copernicus Publications on behalf of the European Geosciences Union.

BGD
12, 5503–5533, 2015

Abstract

This study evaluates three different metrics of vegetation water content estimated from proximal sensing and MODIS satellite imagery: Fuel Moisture Content (FMC), Equivalent Water Thickness (EWT) and Canopy Water Content (CWC). Dry matter (Dm) and Leaf area Index (LAI) were also analyzed in order to connect FMC with EWT and EWT with CWC, respectively. This research took place in a Fluxnet site located in Mediterranean wooded grassland (dehesa) ecosystem in Las Majadas del Tietar (Spain). Results indicated that FMC and EWT showed lower spatial variation than CWC. The spatial variation within the MODIS pixel was not as critical as its temporal trend, so to capture better the variability, fewer plots should be sampled but more times. Due to the high seasonal Dm variability, a constant annual value would not work to predict EWT from FMC. Relative root mean square error (RRMSE) evaluated the performance of nine spectral indices to compute each variable. VARI provided the worst results in all cases. For proximal sensing, GEMI worked best for both FMC (RRMSE = 34.5 %) and EWT (RRMSE = 27.43 %) while NDII and GVMI performed best for CWC (RRMSE = 30.27 % and 31.58 % respectively). For MODIS data, results were a bit better with EVI as the best predictor for FMC (RRMSE = 33.81 %) and CWC (RRMSE = 27.56 %) and GEMI for EWT (RRMSE = 24.6 %). To explain these differences, proximal sensing measures only grasslands at nadir view angle, but MODIS includes also trees, their shades, and other artifacts at up to 20° view angle. CWC was better predicted than the other two water content variables, probably because CWC depends on LAI, which is highly correlated to the spectral indices. Finally, these empirical methods outperformed FMC and CWC products based on radiative transfer model inversion.

BGD
12, 5503–5533, 2015

1 Introduction

Water in leaves is a limiting factor for different physiological processes of vegetation and its deficit causes malfunctioning of different cellular processes. Water is involved in the thermal regulation of plant trough transpiration and also becomes crucial in the uptake of CO_2 for photosynthesis (Chaves et al., 2003). It is also fundamental to maintain turgor pressure, which controls different functional processes of plants like cell enlargement or gas exchange (Taiz and Zeiger, 2010).

Different metrics quantify vegetation water content. Fuel Moisture Content (FMC) (Desbois et al., 1997), defined as the mass of water per unit mass of vegetation, has been extensively used to estimate the fire risk occurrence and fire propagation (García et al., 2008; Yebra et al., 2008b). Equivalent Water Thickness (EWT) or Leaf Water Content (LWC), defined as the mass of water per leaf area, measures the thickness of the water layer with the same leaf area (Danson et al., 1992). Several studies showed that EWT can be retrieved from spectral information at leaf level as it is directly related to the water absorption depth of leaves (Ceccato et al., 2001; Datt, 1999). FMC and EWT are related each other since EWT can be expressed as FMC multiplied by the dry matter (Dm) and divided by 100. Dm is defined as the ratio of leaf dry weight and leaf area (Bowyer and Danson, 2004; Chuvieco et al., 2003). Finally, another metric is the Canopy Water Content (CWC), the mass of water in the canopy per ground area (Cheng et al., 2008; Trombetti et al., 2008). Therefore, CWC represent the product of EWT and Leaf Area Index (LAI), offering not just information at leaf level but at canopy level.

Field sampling of FMC, EWT or CWC relies usually on gravitational methods but this method is quite limited for estimates at regional to global spatial scales, since it requires interpolation to bridge the gaps in both time and space. Remote sensing is a powerful alternative data source to provide information on vegetation water content as it fills such temporal and spatial gaps. Monitoring vegetation water content with remote sensing benefits agriculture, to control crop production and prevent stress in plants (Peñuelas

BGD
12, 5503–5533, 2015

et al., 1992; Sepulcre-Cantó et al., 2006) and forestry, to assess fire danger associated with vegetation water conditions (Chuvieco et al., 2003, 2004; García et al., 2008; Yebra et al., 2008b).

To estimate plant water content with remote sensing, vegetation spectral reflectance has been primarily related to specific water absorption bands in the Short Wave Infrared region (SWIR, 1300–2500 nm) (Ceccato et al., 2001; Zarco-Tejada et al., 2003). Other studies related vegetation water content to spectral indices that do not include SWIR data. These indices monitor the vegetation water content by indirectly relating it to another biophysical parameter that is used as a proxy of water stress. This is the case of the Normalized Difference Vegetation Index (NDVI) (Tucker, 1979), with bands in the Visible (VIS) and Near Infrared (NIR) spectral region, that has shown a close relationship between vegetation biomass, chlorophyll and water content in grasslands (Chuvieco et al., 2003, 2004; García et al., 2008; Yebra et al., 2008b). Least squares regression models have served to empirically relate observed measurements of water content to spectral indices. These models have their weakest point of being site dependent, requiring long datasets for calibration (Chuvieco et al., 2009) and showing different results when the models are extrapolated to other sites using different data sets, making difficult their applicability (Riaño et al., 2005; Yebra et al., 2008a).

Radiative Transfer Models (RTM) simulate vegetation spectra and are a sound alternative to empirical modeling. They can be applied to different locations to estimate different vegetation parameters, as long as the RTM is a true representation of the vegetation canopy. For example, Trombetti et al. (2008) predicted CWC for the continental US using RTM PROSAILH (Baret et al., 1992) simulations. Their model was calibrated with CWC from AVIRIS hyperspectral water absorption bands. Another example is Jurdao et al. (2013) who inverted the RTM GEOSAIL (Huemmrich, 2001) to estimate FMC that was validated with extensive field sampling in Spain.

This study compares the model performance using empirical relationships between three different metrics of vegetation water content (FMC, EWT, CWC) and nine spectral indices calculated from both proximal sensing and MODIS data. Dm and LAI were

BGD
12, 5503–5533, 2015

also analyzed in order to connect FMC with EWT and EWT with CWC, respectively. Firstly, an analysis of the temporal and spatial variability of the different measurements collected in the field was conducted to evaluate which biophysical parameter offers more information. Secondly, the model performance was evaluated to select the most accurate models. Finally, these empirical models were compared to two RTM based models, one to estimate FMC (Jurdao et al., 2013) and the other for CWC (Trombetti et al., 2008).

2 Methods

2.1 Site description

The study site is located at Las Majadas del Tiétar (Spain) FLUXNET site (http://fluxnet.ornl.gov/site/440, last accessed 05 June 2014) (Fig. 1). The area is a *dehesa*, a Mediterranean wooded grassland, which is an ecosystem that occupies about 4 % (2.5 Mha) of the Iberian Peninsula (Castro, 1997). Common tree species are different varieties of oaks, here mostly *Quercus ilex* ssp. *ballota* (L.), whose acorns and leaves are mainly used as forage for pigs and cows, respectively. The scattered oak trees have a 9 m mean height and 6 m mean crown diameter. Due to its deep and wide root system, this species is resistant to long drought periods (Camarero et al., 2012). Short grassland covers 86 % of the area that is managed for cow shepherding. It is mainly composed by *Rumex acetosella* L., *Plantago carinata Schrad, Trifolium subterraneum* L., *Cynodon dactylon* (L.) Pers., *Taraxacum dens-leonis* Desf. and *Vulpia myuros* (L.) C. C. Gmel. During the summer, grassland dries out rapidly and turns into dead matter. Summers are hot and dry, with 30 °C daily average temperature and only 67 mm total precipitation, which are not representative of mean annual 16.7 °C and 572 mm. The average altitude is 256 m above mean sea level. Soils are lixisols with an average thickness of 80 cm. Due to the presence of a clay layer in some of the areas, small water pools may appear in winter after rainy periods. The occurrence of this type

BGD
12, 5503–5533, 2015

of ecosystem in Mediterranean areas worldwide, the need to track the responses to water stress conditions, together with the presence of a FLUXNET eddy covariance flux tower justifies the selection of this site.

2.2 Field sampling

2.2.1 Vegetation sampling

Grasslands water status was destructively sampled every two weeks from April 2009 to April 2011 assuring no rain occurred in the two previous days to avoid sampling superficial water on the leaves. During the summer, grasslands become completely dry and samples were not collected in 2009. However, to ensure the time series continuity of at least one phenological cycle, sampling was restated throughout the summer of 2010. This strategy leaded to a total of 21 valid sampling days for the whole study period.

Six 25 m × 25 m plots were randomly located within the 500 m MODIS pixel that contained the eddy covariance flux tower (Fig. 1). Three grassland samples were collected from three 25 cm × 25 cm quadrants randomly positioned within each plot. Rooted grasses were collected inside the quadrant using clippers. Additionally, a smaller sample was collected outside of the quadrant but nearby to estimate EWT – EWT_{Sample} hereafter – in a cost-effective way, containing a representative proportion of surrounding species. All samples were placed in sealed plastic bags, weighed on a scale with 0.01 g precision and then transported in a cooler to the laboratory. Each EWT_{Sample} and a sub-sample from each quadrant were scanned at 150 pixels per inch (ppi) in an Epson Perfection V30 color scanner (Epson American Inc., Long Beach, CA, USA). Leaf area was calculated automatically from the scanned images using the unsupervised classification algorithm ISOCLUS with 16 iterations in PCI Geomatica (PCI Geomatics, Richmond Hill, Ontario, Canada). All samples were then placed in an oven for 48 h at a constant temperature of 60 °C to obtain their dry weigh. Five biophysical variables were obtained from the collected vegetation samples: FMC, EWT, Dm, CWC and LAI.

BGD
12, 5503–5533, 2015

FMC was determined from the fresh and dry weights of both the whole quadrant sample (FMC_Q) and the EWT_{Sample} (FMC_E) according to Eq. (1)

$$FMC(\%) = \frac{W_{Fresh} - W_{Dry}}{W_{Dry}} \cdot 100 \quad (1)$$

where W_{Fresh} is the fresh weight of the sample measured in the field and W_{Dry} is the oven dried weight.

The EWT_{Sample} permitted to calculate both, EWT and Dm, since fresh/dry weight and leaf area were all measured (Eq. 2):

$$EWT(g\,cm^{-2}) = \frac{W_{Fresh} - W_{Dry}}{Area_{Leaf}} \quad (2)$$

$$Dm(g\,cm^{-2}) = \frac{W_{Dry}}{Area_{Leaf}} \quad (3)$$

where $Area_{Leaf}$ is the leaf area of the EWT_{Sample}.

CWC was calculated from two different approaches. In the first one, quadrant and EWT_{Sample} were combined using the following expression (Eq. 4):

$$CWC_{EWT}(g\,cm^{-2}) = EWT_{Sample} \cdot LAI \quad (4)$$

where LAI is the leaf area index of the grass within the quadrant and EWT is obtained from Eq. (2).

The grass height was very short due to cow shepherding, so LAI, rather than optically estimated, was measured with gravitational methods (He et al., 2007). The biomass to leaf area ratio of a sub-sample inside the quadrant to the total quadrant's biomass provided LAI using the following expression (Eq. 5):

$$LAI(cm^2\,cm^{-2}) = \frac{\frac{W_{Dry}}{W_{Dry}^{Sub}} Area_{Leaf}^{Sub}}{Area} \quad (5)$$

BGD
12, 5503–5533, 2015

where W_{Dry} is the total dry weight of the whole sample inside the quadrant, W_{Dry}^{Sub} is the dry weight of a sub-sample of W_{Dry}, $Area_{Leaf}^{Sub}$ is the sub-sample leaf area and Area is the total area of the quadrant.

The second approach measured CWC from the fresh and dry weight difference inside the quadrant (CWC_Q in Eq. 6):

$$CWC_Q(g\,cm^{-2}) = \frac{W_{Fresh} - W_{Dry}}{Area} \quad (6)$$

2.2.2 Proximal sensing

Simultaneously to vegetation sampling, proximal sensing data were acquired using an ASD FieldSpec® 3 spectroradiometer (http://www.asdi.com/) along NE–SW and NW–SE transects in each 25 m × 25 m plot. This instrument measures reflectance from 350 to 2500 nm. Before measuring along each transect, dark current was recorded, instrument settings were optimized and reference spectra were acquired using a Spectralon® 99 % reflective reference panel (Labsphere Inc., North Sutton, NH, USA). All measurements were taken under clear sky within about ±2 h from local solar noon, to guarantee homogeneous illumination and maximum solar irradiance. Sky conditions were recorded in the field logs, and a quality control check removed the spectra where illumination changes may have occurred after calibration. The ASD was handled without fiber optics to reduce the directional effects on the spectroradiometer's fiber bundle field of view (FOV) (MacArthur et al., 2012). Spectra were acquired at approximately 1.2 m height, rendering a sensor footprint diameter of about 53 cm, since nominal FOV is 25°.

An average of approximately 10 spectral measurements was calculated for each transect and then spectrally resampled to MODIS bands using ITT ENVI 4.7. (EXELIS, Boulder CO, USA). These bands were turned into spectral indices, according to the equations in Table 1. The indices selected to estimate the biophysical variables included bands in the water absorption SWIR region (Faurtyot and Baret, 1997) and

BGD
12, 5503–5533, 2015

bands sensitive to vegetation greenness in the NIR region (Paltridge and Barber, 1988; Yebra et al., 2008b). Finally, two RTM based algorithms were run to compare with these spectral indices. GEOSAIL RTM model inversion estimated FMC testing two different look up tables that constrained the simulations to either a grassland or a mixed tree-grassland cover based on Jurdao et al. (2013). PROSAILH RTM model inversion predicted CWC assuming a pure grassland cover following Trombetti et al. (2008). This model applies the same look up table to all land covers but different calibration coefficients which will render the same R2 independently of the land cover considered.

2.3 MODIS data

MODIS Terra daily surface reflectance (MOD09GA) data from 1 April 2009 to 15 April 2011 were downloaded from NASA Land Processes Distributed Active Archive Center (LP DAAC) at the USGS/Earth Resources Observation and Science (EROS) Center, Sioux Falls, South Dakota, USA. This product includes the reflectance of bands 1 to 7, from 469 to 2130 nm at 500 m spatial resolution, as well as sensor and solar observation angles and quality flags at 1 km. A script programmed in Matlab (Mathworks, Batick, Massachusetts, USA) extracted the MODIS pixel value of our study site from all the images to build the time series. The impact of angular effects on reflectance was reduced by removing images with sensor zenith angles wider than 20°, which also assures the accuracy of the geometrical location of the pixel (Wolfe et al., 2002). In addition, the quality flag layer eliminated images under clouds, cloud shadows and/or with high atmospheric aerosol content. The algorithm selected the closest valid MODIS image to the field sampling day within +5 day window, or the MODIS image acquired before the sampling day in case they were equal. Minimal time lag between sensor and field data reduces the chances of discrepancy, as grassland grazing could affect LAI in a short period of time. This leaded to a total of 14 days of MODIS data with coincident proximal sensing measurements and field data. Similarly to proximal sensing, MODIS estimated the biophysical variables from the spectral indices in Table 1 and from the RTM model inversions.

BGD
12, 5503–5533, 2015

2.4 Data analysis

Intra-group, inter-group and overall R^2 values between FMC_Q, FMC_E, EWT, CWC_Q, CWC_E or LAI, and each of the proximal sensing spectral indices were calculated to investigate their variability within the 500 m MODIS pixel. More specifically, the intra-group R^2 offers information about the spatial variability, due to the collection of samples at different plots within the MODIS pixel. A linear regression model was created for each sampling day where the biophysical variable and the spectral index were the dependent and the independent variable, respectively. The average R^2 of all the regression models for each day provided the intra-group R^2. Instead, the inter-group R^2 explains the temporal variability due to the collection of the samples on different days. In this case, the biophysical variable and the spectral index for all plots were averaged for each day. The linear regression model of these averaged values determined the inter-group R^2. To explain temporal and spatial variability together, the overall R^2 fitted in a single regression model including all plots and sampling days for each spectral index and biophysical variable.

Later, using the mean values of each biophysical variable and the proximal sensing spectral indices, a univariate linear regression model was applied. The same procedure was repeated for MODIS data. Bootstrapping techniques evaluated the empirical model robustness, which is a valid alternative to traditional leave-one-out methods to validate regression models predictability according to Richter et al. (2012). Root Mean Square Error (RMSE), Relative Root Mean Square Error (RRMSE), Nash–Sutcliffe Efficiency index (NSE), determination coefficient (R^2) and Taylor's diagrams evaluated the models' performance. As recommended in Steyerberg et al. (2001), two hundred bootstrap model simulations were run for each model and the median value of each statistics represented its performance. The RMSE measured the error in the estima-

BGD
12, 5503–5533, 2015

tion of the biophysical variable by each model:

$$\mathrm{RMSE} = \sqrt{\frac{1}{n}\sum_{i=1}^{n}\left(V_{\mathrm{est}}^{i} - V_{\mathrm{obs}}^{i}\right)} \tag{7}$$

where V_{est}^{i} is the estimated variable and V_{obs}^{i} is its observed field measurement. RMSE cannot compare the error of different variables with different units. To address this limitation in order to compare the model performances between different variables, RRMSE divides RMSE by the average of the observed values $\overline{V}_{\mathrm{obs}}$ (Richter et al., 2012):

$$\mathrm{RRMSE} = 100\frac{\mathrm{RMSE}}{\overline{V}_{\mathrm{obs}}} \tag{8}$$

The NSE indicates the model predictive power which ranges from $-\infty$ to the best predictive power value of 1 (Richter et al., 2012). It establishes if the model performs at least as accurate as the average of observed values through the following expression:

$$\mathrm{NSE} = 1 - \frac{\sum_{i=1}^{n}\left(V_{\mathrm{est}}^{i} - V_{\mathrm{obs}}^{i}\right)^{2}}{\sum_{i=1}^{n}\left(V_{\mathrm{obs}}^{i} - \overline{V}_{\mathrm{obs}}^{i}\right)^{2}} \tag{9}$$

The R^2 measures the proportion of variance explained by the model and is calculated as:

$$R^2 = 1 - \frac{\sigma_{\mathrm{r}}^{2}}{\sigma^{2}} \tag{10}$$

where σ_{r}^{2} represents the residual variance and σ^{2} is the variance of the dependent variable.

BGD
12, 5503–5533, 2015

Taylor diagrams allowed the comparison between the spectral indices and the RTM based algorithms of Jurdao et al. (2013) and Trombetti et al. (2008) for FMC and CWC, respectively. In these plots the observed variable and its SD are plotted in the x axes. RMSE is represented as semicircles centered at the observed data. The correlation coefficient (r) is displayed in the azimuthal position. Best models are closer in the plot to the observed measurement; therefore they will have a high r, a low RMSE and a SD similar to the observed values.

3 Results

All variables showed similar temporal evolution with a peak in spring and second minor peak in the fall except Dm (Fig. 2). Dm fluctuated throughout the year and exhibited its highest values in the summer. The 47 % Coefficient of Variation (CV) for Dm was less than for CWC_Q (CV = 95 %), CWC_E (CV = 0.95 %), FMC_Q (CV = 60 %) and FMC_E (CV = 56 %), but higher than for EWT (CV = 38 %). A higher precipitation in the spring of 2010 vs. the previous year translated into higher FMC, CWC and LAI values. FMC_E and CWC_E, calculated from the EWT_{Sample}, presented similar trends but in some cases higher values than FMC_Q and CWC_Q, calculated from the quadrant sample.

A low intra-group R^2 for all the variables indicates a low spatial variability between plots (Fig. 3). Contrary, the high inter-group R^2 also for all variables points to the high temporal variability between sampling dates. The main differences between variables occurred for overall R^2. Similar overall and inter-group R^2 values for CWC_E and FMC_E indicated that the combination of the temporal and spatial factors matched in importance each factor on its own. Instead, overall R^2 for CWC_Q and FMC_Q laid in between the inter-group and the intra-group R^2 underling the temporal factor as the main source of variation. GEMI offers the best R^2 for all variables while VARI had the weakest R^2.

The most accurate univariate empirical bootstrap model to retrieve each variable differed from proximal sensing (Fig. 4) to MODIS (Fig. 5). FMC_E and FMC_Q showed the best correlations with GEMI from proximal sensing data but EVI performed better

BGD
12, 5503–5533, 2015

from MODIS. EWT was more accurately estimated with GEMI from either sensor but presented the lowest R^2 and NSE of all the biophysical variables. NDII and GVMI were the most accurate predictors for LAI, CWC_E and CWC_Q with proximal sensing. When using MODIS, the most accurate results for LAI were achieved with NDII and GVMI, but EVI did so for CWC_E and CWC_Q. When the quadrant sample was used instead of the EWT_{Sample}, both FMC and CWC showed more accurate results with lower RRMSE and higher NSE and R^2.

Figures 6 and 7 compare spectral indices and RTM using the Taylor diagrams. In the case of FMC_Q from proximal sensing (Fig. 6), RTM presented higher RMSE and lower r than the spectral indices whereas RTM SD was more similar to the observed values. In the case of FMC_Q estimated from MODIS (Fig. 6), RTM was closer to the empirical models. For CWC_Q (Fig. 7), the RTM from proximal sensing overestimated the SD of the observed CWC_Q. At MODIS scale (Fig. 7), RTM showed a very high overestimation of the CWC_Q.

Temporal evolution of the biophysical variables estimated using the most accurate model for proximal sensing and MODIS in Figs. 4 and 5 are shown in Fig. 6. Both sensors predicted well EWT, FMC_Q and FMC_E but showed an overestimation, especially during the dry season. Contrary, the models for LAI, CWC_E and CWC_Q adjusted well even during the dry season.

4 Discussion

Results revealed that Dm varies significantly throughout the year (CV = 47 %) with high values in the summer. These changes could be related to the temporal variation in plant community structure, species composition and diversity in this ecosystem (Casado et al., 1986). Summer should be the best time of the year to invert RTM and predict Dm, since leaves are drier and therefore EWT does mask the Dm spectral absorption signal (Riano et al., 2005). Casas et al. (2014) applied a constant annual Dm value from the literature to successfully predict seasonal variations in EWT and CWC.

BGD
12, 5503–5533, 2015

However, our study suggests that, due to the high seasonal variation in Dm, a constant annual value would not be recommended here.

The high inter-group and low intra-group R^2 implies that the temporal trend is much more critical than the spatial variation within the MODIS pixel (Fig. 3). Therefore, the strategy to capture better the variability of vegetation water content in this ecosystem should be to sample more times but fewer plots. In addition, CWC_Q and FMC_Q, generated from larger sample sizes than CWC_E and FMC_E, presented higher inter-group R^2 values, which indicate a better characterization of the temporal variability. This suggests the need to standardize sampling protocols for the estimation of vegetation biophysical parameters to ensure data quality, repeatability and to facilitate accurate cross comparison from different studies. Some initiatives already exist to facilitate this standardization, as the Global Terrestrial Carbon System (GTOS) guidelines in support of carbon cycle science (Law et al., 2008). However, currently there is no international backbone that ensures this and an agreement in the protocols is needed in order to validate remote sensing products.

CWC was better predicted than the other two water content variables, FMC and EWT (Fig. 3). CWC depends on LAI which is even higher correlated than those two variables. It is possible to have the same FMC and EWT for different LAI and hence different CWC and amount of soil background, which will change its reflectance. Yebra et al. (2013) demonstrated through PROSAILH simulations how a very different CWC for the same EWT based on changes of LAI translates into a huge range of NDII values. Our results confirm this theoretical assumption described in Yebra et al. (2013). This issue is especially critical over areas like this one with large dynamic annual growth.

The empirical methods estimated FMC and CWC with slightly different results for proximal sensing and MODIS (Figs. 4 and 5). While GEMI and NDII were the most accurate for FMC and CWC respectively from proximal sensing in our study; EVI was the most accurate estimator of both variables from MODIS. In addition, it is remarkable that MODIS estimations were more accurate than proximal sensing. Roberts et al. (2006) also observed different correlations between indices and platforms and the discrep-

BGD
12, 5503–5533, 2015

ancies here need further investigation. The MODIS pixel included not only grasslands but also trees, their shades, and other marginal covers like bare soil and a water pond (Fig. 1), and its view angle could be up to 20°. Proximal sensing measures only two transects within each of the six plots and provides only nadiral measurements which could be more affected by the soil signal.

Similarly to this study, Casas et al. (2014) reliably predicted water content variables in California (USA) from GEMI, NDII and EVI using simulated MODIS spectral response from airborne hyperspectral AVIRIS instrument. In their case, it was actually VARI the most accurate for grasslands (FMC and CWC), chaparral (EWT, FMC and CWC) and a Mediterranean oak forest (EWT). Contrary, VARI showed very poor accuracies in our case to estimate FMC, EWT and CWC, but was still capable of capturing the variability in LAI (Fig. 3). This fact also contradicts other studies that predicted FMC from VARI on chaparral (Peterson et al., 2008; Roberts et al., 2006; Stow et al., 2005, 2006). VARI was developed to detect vegetation fraction in homogenous wheat crops (Gitelson et al., 2002b), but Gitelson et al. (2002a) nor the above studies have tested this spectral index to detect vegetation water content on sites like ours, with strong seasonal changes in species composition and LAI.

The empirical methods calibrated for this specific site outperformed the physical RTM estimates for CWC and FMC (Figs. 4 and 5). This confirms the results in Casas et al. (2014) where the CWC algorithm based on RTM inversion developed by Trombetti et al. (2008) also failed to improve results from empirical estimates. RTM only overcome empirical approaches when structural information constrains the model inversion (Yebra et al., 2008b; Casas et al., 2014). Such ancillary information is key to successfully extrapolate a RTM inversion at broader scale.

5 Conclusions

This work showed a complete analysis of three metrics, EWT, FMC and CWC, to measure vegetation water content at two different spatial scales by using proximal sensing

BGD
12, 5503–5533, 2015

from a field spectroradiometer and MODIS images. The temporal changes in these metrics are more critical than their spatial variation within the MODIS pixel. Results indicated that larger samples collected using quadrants are more representative than the small EWT_{Sample} in order to follow the temporal trends in FMC and CWC. Protocol standardization in order to make different datasets comparable should be considered to make different dataset comparable both spatially and temporally. Due to the high seasonal Dm variability, a constant annual value should not be used to estimate EWT from FMC in this ecosystem. The dependence of CWC on LAI makes this vegetation water content variable easier to predict than FMC or EWT.

GEMI, NDII and EVI reliably predicted vegetation water content. The best empirical estimator differed between sensors. Results were a bit better for MODIS than proximal sensing, probably due to differences in view angles, sampling strategy and canopy observed. These empirical methods still exceed RTM inversions developed for other sites to predict FMC (Jurdao et al., 2013) and CWC (Trombetti et al., 2008).

Acknowledgements. This study has been carried out in the context of the BIOSPEC (CGL2008-02301) and FLUXPEC (CGL2012-34383) projects funded by the Spanish Ministry of Science and Innovation and the Ministry of Economy and Competiveness respectively. The FPI grant program supported Gorka Mendiguren predoctoral research (BES-2009-026831) as well as short stays at the University of Copenhagen during year 2011 (EEBB-2011-44463) and 2012 (EEBB-I-12-04542) and to Rasmus Fensholt for hosting in the department. All the people involved in the field work campaigns from different institution: Spanish Council for Scientific Research, University of Alcalá de Henares, University of Zaragoza, CEAM and Instituto Nacional de Investigaciones Agrarias (INIA) are acknowledged. Collaboration with NASA Terrestrial Hydrology Program (grant # NNX09AN51G) and David Riaño for his comments and suggestions are also acknowledged. The first author would like to thank Spanish INEM for its funding support.

cost EUROPEAN COOPERATION IN SCIENCE AND TECHNOLOGY

This publication was supported by COST – www.cost.eu

BGD
12, 5503–5533, 2015

References

Baret, F., Jacquemoud, S., Guyot, G., and Leprieur, C.: Modeled analysis of the biophysical nature of spectral shifts and comparison with information content of broad bands, Remote Sens. Environ., 41, 133–142, 1992.

Bowyer, P. and Danson, F. M.: Sensitivity of spectral reflectance to variation in live fuel moisture content at leaf and canopy level, Remote Sens. Environ., 92, 297–308, 2004.

Camarero, J. J., Olano, J. M., Arroyo Alfaro, S. J., Fernández-Marín, B., Becerril, J. M., and García-Plazaola, J. I.: Photoprotection mechanisms in *Quercus ilex* under contrasting climatic conditions, flora: morphology, distribution, Funct. Ecol. Plant., 207, 557–564, 2012.

Casado, M. A., de Miguel, J. M., Sterling, A., Peco, B., Galiano, E. F., and Pineda, F. D.: Production and spatial structure of Mediterranean pastures in different stages of ecological succession, Vegetatio, 64, 75–86, doi:10.1007/BF00044783, 1986.

Casas, A., Riaño, D., Ustin, S. L., Dennison, P., and Salas, J.: Estimation of water-related biochemical and biophysical vegetation properties using multitemporal airborne hyperspectral data and its comparison to MODIS spectral response, Remote Sens. Environ., 148, 28–41, doi:10.1016/j.rse.2014.03.011, 2014.

Castro, E. B.: Los Bosques Ibéricos: Una Interpretación Geobotánica, Editorial Planeta, Barcelona, S. A., 1997.

Ceccato, P., Flasse, S., Tarantola, S., Jacquemoud, S., and Grégoire, J.-M.: Detecting vegetation leaf water content using reflectance in the optical domain, Remote Sens. Environ., 77, 22–33, 2001.

Ceccato, P., Gobron, N., Flasse, S., Pinty, B., and Tarantola, S.: Designing a spectral index to estimate vegetation water content from remote sensing data, part 1. Theoretical approach, Remote Sens. Environ., 82, 188–197, 2002.

Chaves, M. M., Maroco, J. P., and Pereira, J. S.: Understanding plant responses to drought from genes to the whole plant, Functional. Plant. Biology., 30, 239–264, doi:10.1071/FP02076, 2003.

Cheng, Y.-B., Ustin, S. L., Riaño, D., and Vanderbilt, V. C.: Water content estimation from hyperspectral images and MODIS indexes in Southeastern Arizona, Remote Sens. Environ., 112, 363–374, 2008.

BGD
12, 5503–5533, 2015

Chuvieco, E., Aguado, I., Cocero, D., and Riaño, D.: Design of an empirical index to estimate fuel moisture content from NOAA-AVHRR images in forest fire danger studies, Int. J. Remote Sens., 24, 1621–1637, 2003.

Chuvieco, E., Cocero, D., Riaño, D., Martin, P., Martínez-Vega, J., de la Riva, J., and Pérez, F.: Combining NDVI and surface temperature for the estimation of live fuel moisture content in forest fire danger rating, Remote Sens. Environ., 92, 322–331, 2004.

Chuvieco, E., Wagtendok, J., Riaño, D., Yebra, M., and Ustin, S.: Estimation of fuel conditions for fire danger assessment, in: earth observation of wildland fires in Mediterranean ecosystems, Springer, Berlin, Heidelberg, 83–96, 2009.

Danson, F., Steven, M. D., Malthus, T. J., and Clark, J. A.: High-spectral resolution data for determining leaf water content, Int. J. Remote Sens., 13, 461–470, 1992.

Datt, B.: Remote sensing of water content in Eucalyptus leaves, Aust. J. Botany, 47, 909–923, 1999.

Desbois, N., Deshayes, M., and Beudin, A.:Protocol for Fuel Moisture Content Measurements, in: A review of remote sensing methods for the study of large wildland fires, Location: Alcalá de Henares, Name of publisher: Departamento de Geografía, Universidad de Alcalá, edited by: Chuvieco, E., 61–72 pp., 1997.

Faurtyot, T. and Baret, F.: Vegetation water and dry matter contents estimated from top-of-the-atmosphere reflectance data: a simulation study, Remote Sens. Environ., 61, 34–45, doi:10.1016/S0034-4257(96)00238-6, 1997.

Gao, B.-C.: NDWI a normalized difference water index for remote sensing of vegetation liquid water from space, Remote Sens. Environ., 58, 257–266, 1996.

García, M., Chuvieco, E., Nieto, H., and Aguado, I.: Combining AVHRR and meteorological data for estimating live fuel moisture content, Remote Sens. Environ., 112, 3618–3627, 2008.

Gitelson, A. A., Kaufman, Y. J., Stark, R., and Rundquist, D.: Novel algorithms for remote estimation of vegetation fraction, Remote Sens. Environ., 80, 76–87, 2002a.

Gitelson, A. A., Stark, R., Grits, U., Rundquist, D., Kaufman, Y., and Derry, D.: Vegetation and soil lines in visible spectral space: a concept and technique for remote estimation of vegetation fraction, Int. J. Remote Sens., 23, 2537–2562, doi:10.1080/01431160110107806, 2002b.

Hardisky, M. A., Klemas, V., and Smart, R. M.: The influence of soil salinity, growth form, and leaf moisture on the spectral radiance of *Spartina alterniflora* canopies, Photogramm. Eng. Rem. S., 49, 77–83, 1983.

BGD
12, 5503–5533, 2015

He, Y., Guo, X., and Wilmshurst, J. F.: Comparison of different methods for measuring leaf area index in a mixed grassland, Can. J. Plant Sci., 87, 803–813, doi:10.4141/cjps07024, 2007.
Huemmrich, K. F.: The GeoSail model: a simple addition to the SAIL model to describe discontinuous canopy reflectance, Remote Sens. Environ., 75, 423–431, doi:10.1016/S0034-4257(00)00184-X, 2001.
Huete, A.: A soil-adjusted vegetation index (SAVI), Remote Sens. Environ., 25, 295–309, 1988.
Huete, A., Didan, K., Miura, T., Rodriguez, E. P., Gao, X., and Ferreira, L. G.: Overview of the radiometric and biophysical performance of the MODIS vegetation indices, Remote Sens. Environ., 83, 195–213, 2002.
Jurdao, S., Yebra, M., Guerschman, J. P., and Chuvieco, E.: Regional estimation of woodland moisture content by inverting radiative transfer models, Remote Sens. Environ., 132, 59–70, doi:10.1016/j.rse.2013.01.004, 2013.
Law, B., Arkebauer, T., Campbell, J., Chen, J., Sun, O., Schwartz, M., van Ingen, C., and Verma, S.: Terrestrial carbon observations: protocols for vegetation sampling and data submission, Terrestrial Carbon Observations Panel of the Global Terrestrial Observing System, FAO, Rome, Italy, 2008.
MacArthur, A., MacLellan, C. J., and Malthus, T.: The fields of view and directional response functions of two field spectroradiometers, IEEE T. Geosci. Remote, 50, 3892–3907, doi:10.1109/tgrs.2012.2185055, 2012.
Paltridge, G. W. and Barber, J.: Monitoring grassland dryness and fire potential in australia with NOAA/AVHRR data, Remote Sens. Environ., 25, 381–394, doi:10.1016/0034-4257(88)90110-1, 1988.
Peterson, S. H., Roberts, D. A., and Dennison, P. E.: Mapping live fuel moisture with MODIS data: a multiple regression approach, Remote Sens. Environ., 112, 4272–4284, doi:10.1016/j.rse.2008.07.012, 2008.
Pinty, B. and Verstraete, M. M.: GEMI: a non-linear index to monitor global vegetation from satellites, Plant Ecol., 101, 15–20, 1992.
Riaño, D., Vaughan, P., Chuvieco, E., Zarco-Tejada, P. J., and Ustin, S. L.: Estimation of fuel moisture content by inversion of radiative transfer models to simulate equivalent water thickness and dry matter content: analysis at leaf and canopy level, IEEE T. Geosci. Remote, 43, 819–826, doi:10.1109/tgrs.2005.843316, 2005.

BGD
12, 5503–5533, 2015

Richter, K., Atzberger, C., Hank, T. B., and Mauser, W.: Derivation of biophysical variables from Earth observation data: validation and statistical measures, APPRES, 6, 063557-063551–063557-063523, doi:10.1117/1.jrs.6.063557, 2012.

Roberts, D. A., Dennison, P. E., Peterson, S., Sweeney, S., and Rechel, J.: Evaluation of Airborne Visible/Infrared Imaging Spectrometer (AVIRIS) and Moderate Resolution Imaging Spectrometer (MODIS) measures of live fuel moisture and fuel condition in a shrubland ecosystem in southern California, J. Geophys. Res. Biogeosci., 111, G04S02, doi:10.1029/2005jg000113, 2006.

Steyerberg, E. W., Harrell Jr, F. E., Borsboom, G. J. J. M., Eijkemans, M. J. C., Vergouwe, Y., and Habbema, J. D. F.: Internal validation of predictive models: efficiency of some procedures for logistic regression analysis, J. Clin. Epidemiol., 54, 774–781, doi:10.1016/S0895-4356(01)00341-9, 2001.

Stow, D., Niphadkar, M., and Kaiser, J.: MODIS-derived visible atmospherically resistant index for monitoring chaparral moisture content, Int. J. Remote Sens., 26, 3867–3873, doi:10.1080/01431160500185342, 2005.

Stow, D., Niphadkar, M., and Kaiser, J.: Time series of chaparral live fuel moisture maps derived from MODIS satellite data, Int. J. Wildland Fire, 15, 347–360, doi:10.1071/WF05060, 2006.

Taiz, L. and Zeiger, E.: Plant Physiology, Sinauer Associates, Incorporated, Sunderland, 2010.

Trombetti, M., Riaño, D., Rubio, M. A., Cheng, Y. B., and Ustin, S. L.: Multi-temporal vegetation canopy water content retrieval and interpretation using artificial neural networks for the continental USA, Remote Sens. Environ., 112, 203–215, 2008.

Tucker, C. J.: Red and photographic infrared linear combinations for monitoring vegetation, Remote Sens. Environ., 8, 127–150, 1979.

Wolfe, R. E., Nishihama, M., Fleig, A. J., Kuyper, J. A., Roy, D. P., Storey, J. C., and Patt, F. S.: Achieving sub-pixel geolocation accuracy in support of MODIS land science, Remote Sens. Environ., 83, 31–49, doi:10.1016/S0034-4257(02)00085-8, 2002.

Yebra, M., Chuvieco, E., and Aguado, I.: Comparación entre modelos empíricos y de transferencia radiativa para estimar contenido de humedad en pastizales: poder de generalización, Rev. Teledetección, 29, 73–90, 2008a.

Yebra, M., Chuvieco, E., and Riaño, D.: Estimation of live fuel moisture content from MODIS images for fire risk assessment, Agr. Forest Meteorol., 148, 523–536, 2008b.

Yebra, M., Dennison, P. E., Chuvieco, E., Riaño, D., Zylstra, P., Hunt Jr, E. R., Danson, F. M., Qi, Y., and Jurdao, S.: A global review of remote sensing of live fuel moisture content for

BGD
12, 5503–5533, 2015

fire danger assessment: moving towards operational products, Remote Sens. Environ., 136, 455–468, doi:10.1016/j.rse.2013.05.029, 2013.

Zarco-Tejada, P. J., Rueda, C. A., and Ustin, S. L.: Water content estimation in vegetation with MODIS reflectance data and model inversion methods, Remote Sens. Environ., 85, 109–124, 2003.

BGD

12, 5503–5533, 2015

Table 1. Spectral indices calculated using field reflectance measurements and MODIS data.

Index	Formula	Reference
Normalized difference vegetation index (NDVI)	$NDVI = \frac{B_2-B_1}{B_2+B_1}$	(Tucker, 1979)
Enhanced Vegetation Index (EVI)	$EVI = 2.5 \cdot \left(\frac{B_2-B_1}{B_2+6 \cdot B_1-7.5 \cdot B_3}\right)$	(Huete et al., 2002)
Normalized Difference Water Index (NDWI)	$NDWI = \frac{B_2-B_5}{B_2+B_5}$	(Gao, 1996)
Normalized Difference Infrared Index (NDII)	$NDII = \frac{B_2-B_6}{B_2+B_6}$	(Hardisky et al., 1983)
Simple Ratio Water Index (SRWI)	$SRWI = \frac{B_2}{B_5}$	(Zarco-Tejada et al., 2003)
Soil Adjusted Vegetation Index (SAVI)	$SAVI = \left(\frac{B_2-B_1}{B_2+B_1+L}\right) \cdot (1+L)$ Where $L = 0.5$	(Huete, 1988)
Global Environment Monitoring Index (GEMI)	$GEMI = \eta \cdot (1 - -0.25\eta) - \frac{B_1-0.125}{1-B_1}$ where $\eta = \frac{2 \cdot \left(B_2^2-B_1^2\right)+1.5 \cdot B_2+0.5 \cdot B_2}{B_2+B_1+0.5}$	(Pinty and Verstraete, 1992)
Visible Atmospherically Resistant Index (VARI)	$VARI = \frac{B_4-B_1}{B_4+B_1-B_3}$	(Gitelson et al., 2002a)
Global Vegetation Monitoring Index (GVMI)	$GVMI = \frac{(NIR_{REC}+0.1)-(SWIR_{REC}-0.02)}{(NIR_{REC}+0.1)+(SWIR_{REC}-0.02)}$	(Ceccato et al., 2002)
Central band wavelength	B1 = 645.5 nm, B2 = 856.5 nm, B3 = 465.6 nm, B4 = 553.6 nm, B5 = 1241.6 nm, B6 = 1629.1 nm, B7 = 2114.1 nm	

BGD
12, 5503–5533, 2015

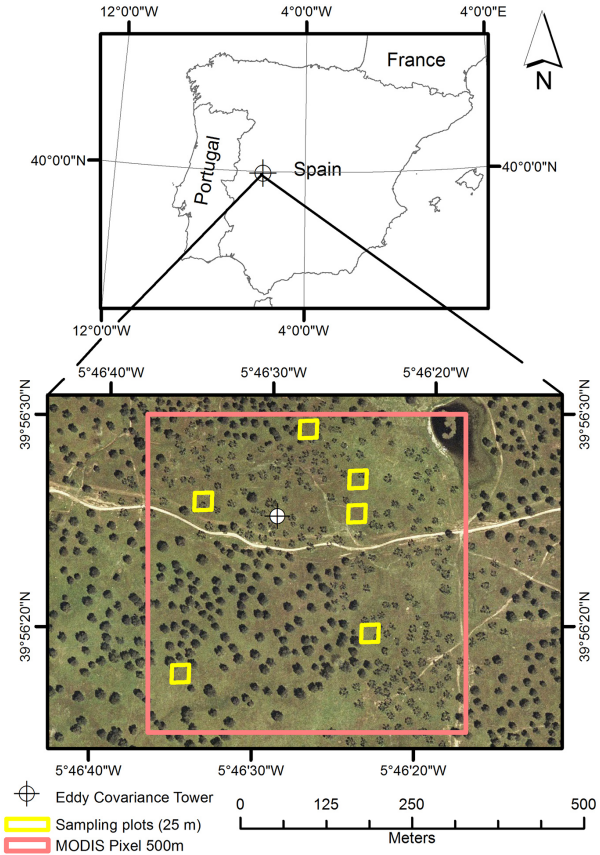

Figure 1. Plots sampled near the FLUXNET tower within the 500 m MODIS pixel at Las Majadas del Tiétar (Spain) study site.

BGD
12, 5503–5533, 2015

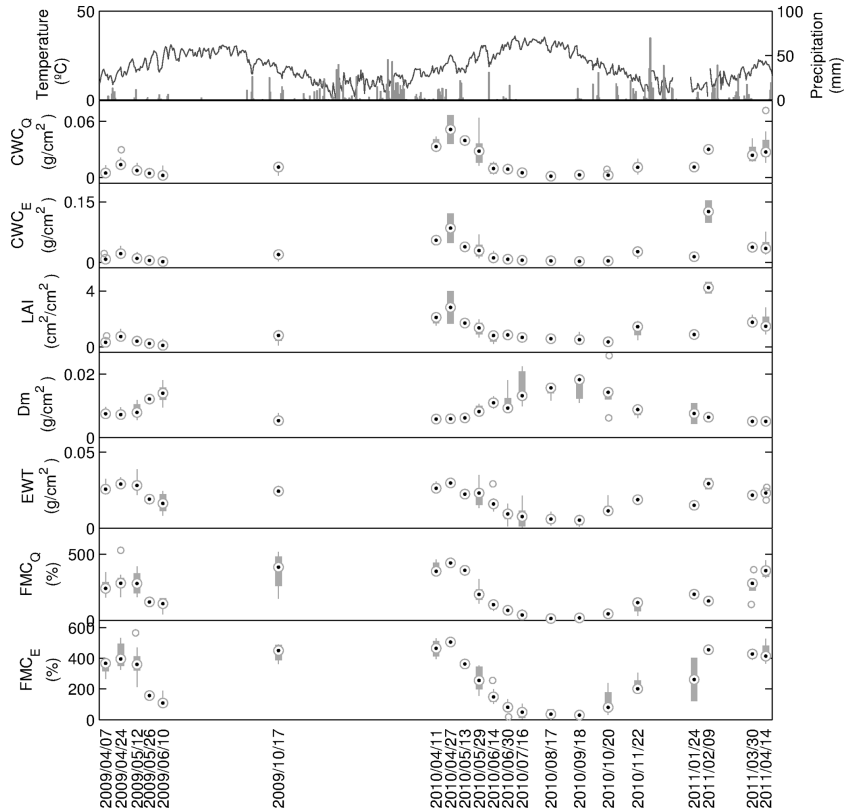

Figure 2. Box plot showing the temporal evolution of field biophysical variables measured. Filled points represent the median of the daily measurements, the boxes indicate the position of the 1st and 3rd quartile, lines delimit the maximum and minimum values, and empty points are outliers. Precipitation is represented using bars and temperature is represented with a solid line

BGD
12, 5503–5533, 2015

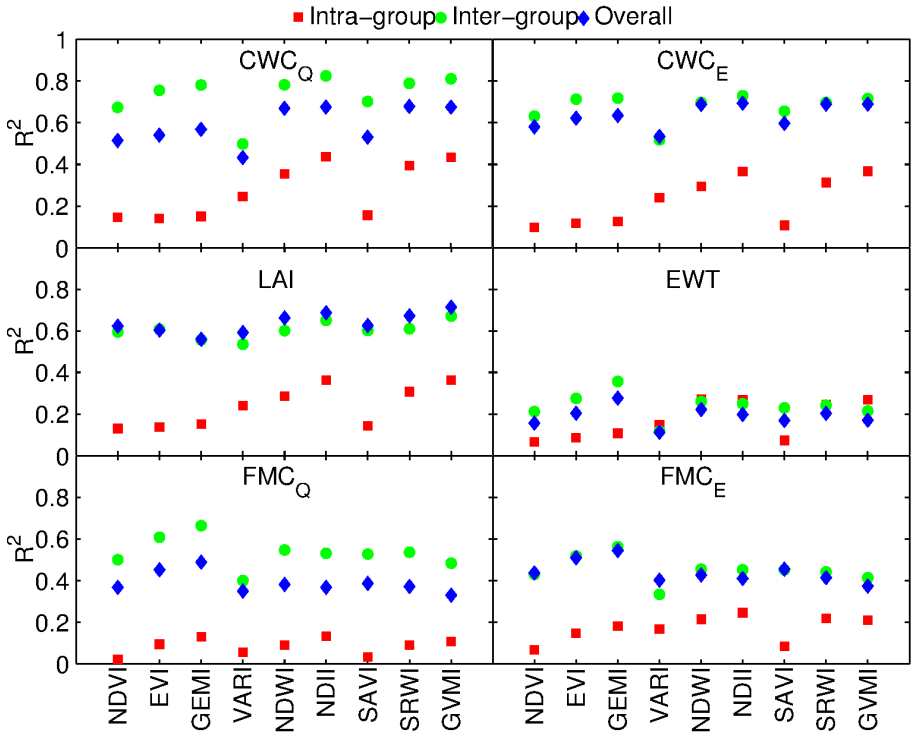

Figure 3. Intra-group, inter-group and overall R^2 values between proximal sensing spectral indexes and biophysical variables measured in the field.

BGD
12, 5503–5533, 2015

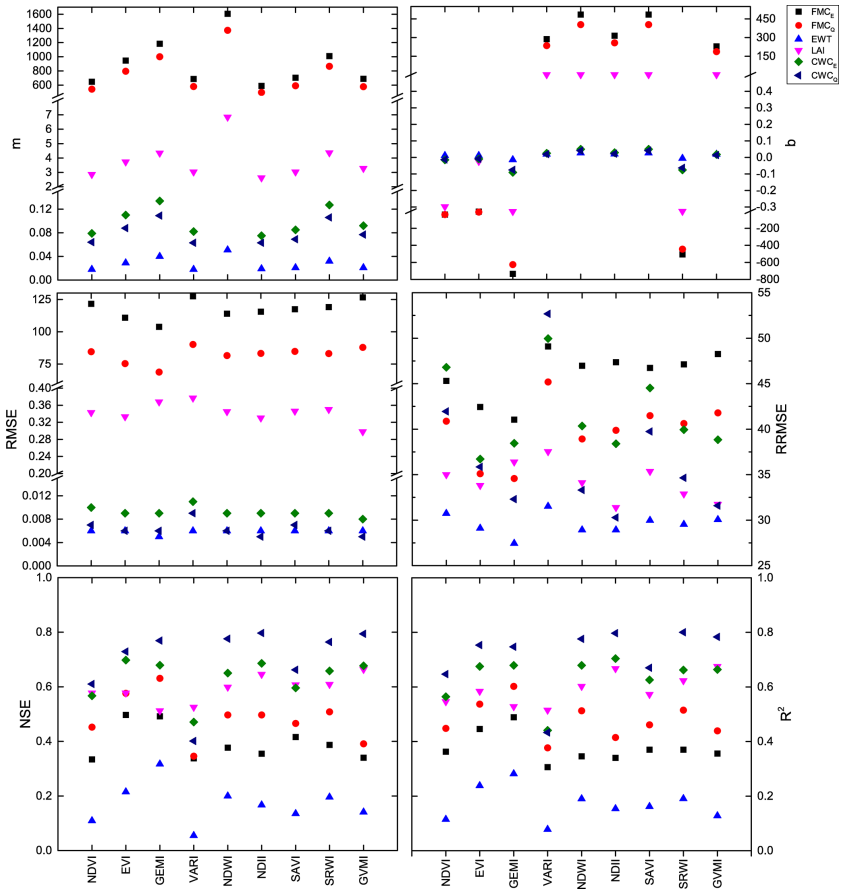

Figure 4. Model performance statistics for all the spectral indices calculated using proximal sensing.

BGD
12, 5503–5533, 2015

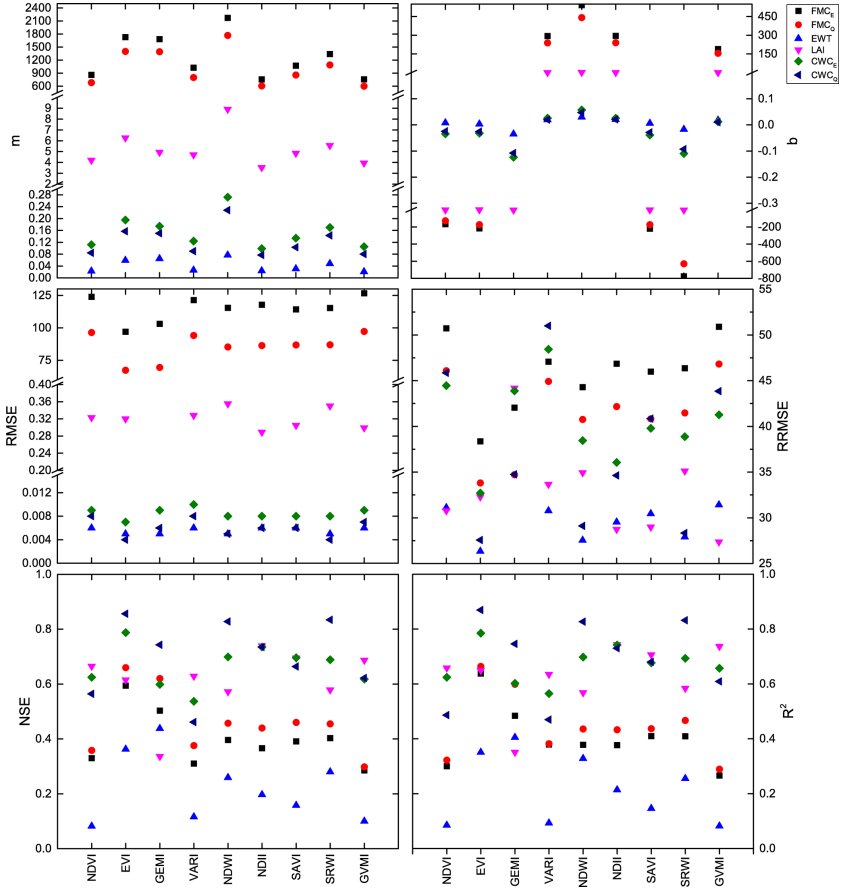

Figure 5. Model performance statistics for all the spectral indices calculated using MODIS data.

BGD
12, 5503–5533, 2015

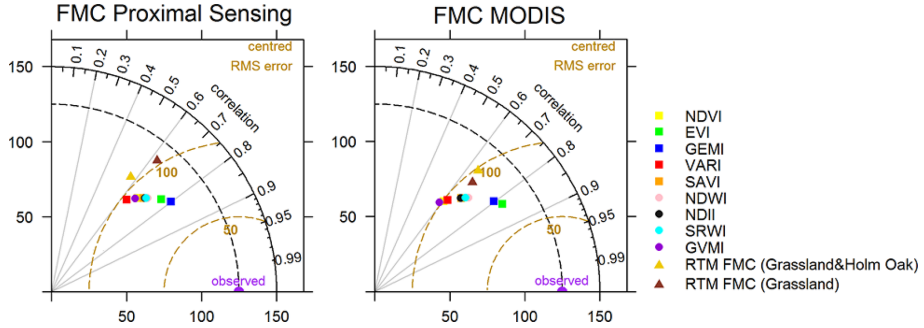

Figure 6. Comparison of empirical vs. RTM models to estimate FMC with proximal sensing (left) and MODIS (right).

BGD
12, 5503–5533, 2015




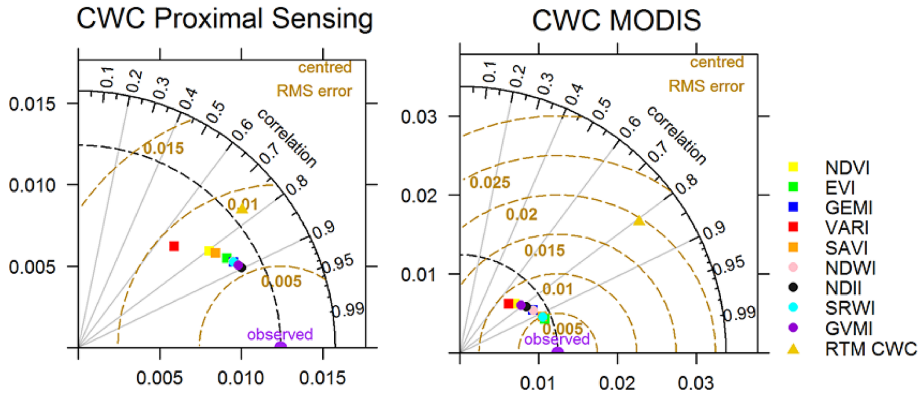

Figure 7. Comparison of empirical vs. RTM models to estimate CWC with proximal sensing (left) and MODIS (right).

BGD
12, 5503–5533, 2015

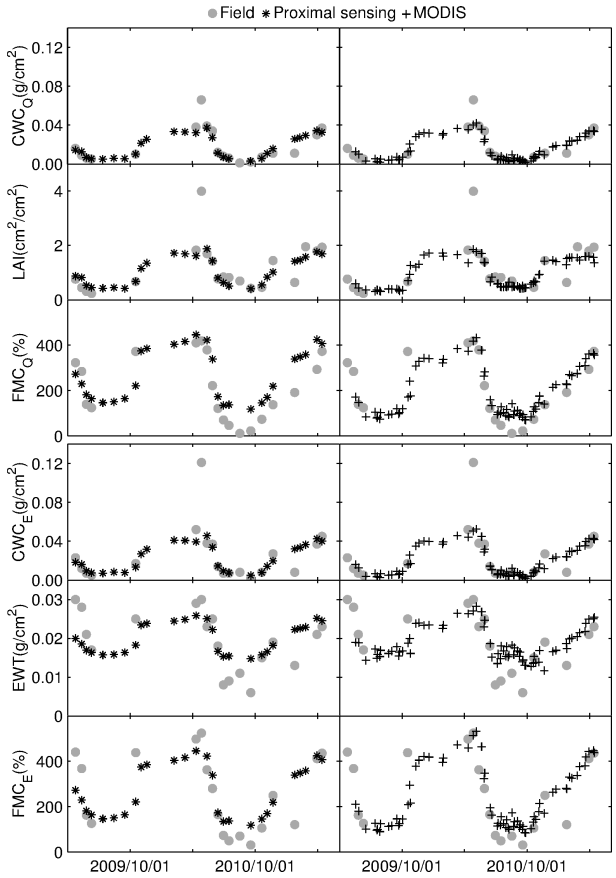

Figure 8. Temporal evolution of the observed (circles) and estimated FMC_E, FMC_Q, EWT, LAI, CWC_E and CWC_Q obtained for proximal sensing (asterisks) and MODIS (crosses).

BGD
12, 5503–5533, 2015